Mosaicing with Even Higher Dynamic Range

M.A. Holdaway

January 22, 1992

1 Introduction

This memo investigates producing mosaic images of sources which are dominated by very bright unresolved features. Much of the work here builds on Braun (1988) in which some of the ideas required for moderately high dynamic range mosaicing are developed.

Consider a bright, unresolved feature surrounded by structure larger than can be measured by the shortest interferometric spacings. While mosaicing and possibly total power measurements are required to image the large scale structure, reconstruction errors from the bright unresolved feature may dominate the image: if maximum entropy mosaicing is used, the sidelobes from the point source will corrupt the large scale structure (Narayan and Nityananda, 1986); pointing errors and errors in the primary beam model will result in inconsistencies in the data taken from different sky positions; and bright sources can seep through the primary beam sidelobes which are beyond the primary beam model used in reconstruction. Inconsistencies in the data from the various pointings on the sky will scatter power about the image, limiting the dynamic range. It would be preferred to isolate any inconsistencies at the location of the bright point sources, resulting only in an error for the flux of the point sources. Various methods for proceeding towards this goal are considered and evaluated. Three variations of the IMERG program and a generalized, automated UVSUB-like scheme are considered in simulations. The simulation results are judged visually, by dynamic range (**DR**), and by fidelity index (**FI**) (Cornwell, Holdaway, and Uson, 1992). The **DR** is the peak signal divided by the rms off-source error, and the **FI** is the representative on-source SNR. Also, a high **DR** (10000:1) mosaic image of NGC253 at 3.6 cm is presented.

2 IMERG

Consider a high resolution image which suffers from short spacing problems and accurately measures the Fourier plane for spacings of u_1 and greater, and a low resolution image which accurately samples the Fourier plane out to u_2, with $u_2 > u_1$. The AIPS task IMERG performs a Fourier transform on each image, scales them appropriately, and generates a new Fourier plane which is equal to the low resolution Fourier plane out to u_1, the high resolution

Fourier plane beyond u_2, and the average value of the two between u_1 and u_2. The final image is obtained by back transforming the new combined Fourier plane.

Using IMERG, one can increase the **DR** of mosaic images and reduce the processing time. First, each field is imaged and deconvolved separately using all baselines, and the appropriate linear combination of the fields, weighted by the primary beam, yields the LTESS image. This high resolution image will accurately represent structure corresponding to baselines greater than u_1, but will not do well reconstructing very extended emission. A low resolution nonlinear mosaic can be made from the short spacings out to u_2, including total power if present. The two images can then be combined in the Fourier plane using IMERG.

3 Alternatives to IMERG

While IMERG works well for moderate **DR**, IMERG introduces ringing into the final images when used on sources which require very high **DR**. The performance of IMERG and its alternatives is explored.

3.1 Different Fourier Plane Recombination Schemes

IMERG assumes there is an annulus in the Fourier plane between u_1 and u_2 over which the low resolution image made by mosaicing short spacings and the high resolution image made by a linear combination of independently deconvolved clean images agree to a high degree, where *high degree* depends upon the required **DR**. IMERG treats the annulus of overlap by averaging the high and low resolution Fourier plane pixel values. Any errors in this range of spatial frequencies can therefore only be reduced by at most a factor of two. The sharp cutoffs in both high and low resolution planes result in ringing at some level if there are any discrepancies between the low and high resolution Fourier planes in the region of overlap. To try to reduce this ringing, a linear and a Gaussian weighted average in the annulus of overlap have been tested (see Figure 1 for illustration). The original IMERG will be referred to as AVE IMERG and the two new schemes will be called LIN IMERG and GAUSS IMERG.

3.2 UVSUB and Mosaicing the Residuals

For sources which have very bright compact features, MEM will often produce unsatisfactory images and there seems to be no escape from using a clean-like algorithm to determine the structure of these features. Once determined by CLEAN, bright unresolved features can be subtracted from the

visibilities. The residual visibilities can then be imaged with a joint mosaic deconvolution. If necessary, the subtracted clean components can be added back in the image plane. MOSCLEAN is a program in SDE which makes dirty maps and cleans them for each pointing, subtracts the clean components which reside in user-specified boxes from the visibilities for each pointing, and combines the subtracted components for all pointings into a single map using the proper primary beam weighting. MOSCLEAN is an automated version of LTESS/UVSUB. For very extended sources, this process of cleaning each field takes a rather long time, and it is important to know how the reconstruction errors depend upon the depth of the cleaning.

The dirty linear mosaic image is a linear combination of the dirty images:

$$I^D_{LM}(\mathbf{x}) = \frac{\sum_p A_p(\mathbf{x}-\mathbf{x}_p) I^D_p(\mathbf{x})}{\sum_p A_p(\mathbf{x}-\mathbf{x}_p)^2}. \tag{1}$$

If we clean down to ϵ, the value of some cleaned pixel will be

$$I^D_{LM}(\mathbf{x}) \leq \frac{\sum_p A_p(\mathbf{x}-\mathbf{x}_p)\epsilon}{\sum_p A_p(\mathbf{x}-\mathbf{x}_p)^2} \simeq 2\epsilon. \tag{2}$$

The increase in the linear mosaic map occurs because nearby pointings will be cleaned only down to ϵ and the primary beam correction will raise the flux of that pixel. The amount of flux which is scattered across the whole map by the error associated with a single point source is approximately the error made in the point source's flux times the rms sidelobe level in the point spread function (PSF), or $\epsilon\sigma_{PSF}$. If there are N bright point-like sources which are all being cleaned and removed from the visibilities, then the flux scattered across the map will be approximately $\sqrt{N}\epsilon\sigma_{SB}$. The **FI** of the final image will go like $S_{median}/(\sqrt{N}\epsilon\sigma_{SB})$ and the **DR** after adding back the convolved clean components, will go like $S_{peak}/(\sqrt{N}\epsilon\sigma_{SB})$. For the proposed MMA, the synthesized beam for a snapshot in the compact configuration will have an rms sidelobe level of about 0.025. This simple analysis predicts the dynamic range found in simulations to within 50%. Of course, for very low ϵ the **DR** will be limited by other factors such as deconvolution errors or thermal noise. Figure 2 illustrates the **DR** and **FI** of the simulated images as a function of clean stopping flux ϵ.

There is another alternative to cleaning all pointings to the same level. As stated above, the errors are due to inconsistencies in the flux estimate of the point sources which are scattered across the image by the synthesized beam. A better job can be done if each field is cleaned down to a level which depends upon the location of the point source in the primary beam for that pointing so that the residual flux of the point source is more consistent among the different pointings. This is problematic if there is more

than one point source in the field. Instead, the clean components need to be altered such that the residual level in the image is roughly constant *after* correcting for the primary beam. Figure 3 illustrates the steps involved. First, a unit mask is made from a single pointing's clean components which have been selected for (u, v) subtraction. (ie, an image which is one at pixels with the clean components and zero elsewhere). This mask is multiplied by the primary beam and scaled by ϵ/β, where β is some fiducial primary beam level (0.2, for example). ϵ is added to the nonzero pixels in the original clean component image, and the processed mask image is subtracted from the original clean component image. The resulting processed clean component image can then be Fourier transformed, degridded, and subtraced from the measured visibilities. This process must be repeated for each observed pointing. When the residual visibilities are mosaiced, the flux estimates at the position of a subtracted point source will be consistent for all pointings for which the point source is above the β primary beam level. Hence, less flux is scattered across the image and the resulting dynamic range is much higher. When the point source is below the β primary beam level, the data are again inconsistent, but at a level which is much lower than the previous paragraph's inconsistent CLEAN/UVSUB method. This consistent method will break down when ϵ/β is greater than the point sources which are being subtracted from the visibilities. An estimate of the level of error caused by processing the data in this way is

$$\frac{\sum_{(p, A_p(\mathbf{x}-\mathbf{x}_p)<\beta)} A_p(\mathbf{x}-\mathbf{x}_p)\epsilon}{\sum_p A_p(\mathbf{x}-\mathbf{x}_p)^2} \sim .1\epsilon. \tag{3}$$

Hence, an inconsistent subtraction method requires much deeper cleaning than a consistent subtraction method to obtain the same **DR**. While this technique seems quite promising, the improvement over inconsistent point source subtraction has only been found to be about a factor of two rather than ten. This is still being investigated.

3.3 Comparison of Methods

Simulations were performed with the current design for the MMA compact configuration (Braun, 1989; Holdaway, 1990). Total power was measured with the interferometric elements in accordance with the homogeneous array design (Cornwell, Holdaway, and Uson, 1992). The model brightness distribution is the M31 image used in previous simulations with either a scaled point source or a scaled 4″ FWHM Gaussian added near the center of the image. (The beam of the compact configuration at 230 GHz is 3.″7.) The peak brightness ranged from 34 Jy/beam when no bright source was added to over 1000 Jy/beam, and there is a wealth of detail in the model image

down to .2 Jy/beam. All Fourier transforms were made onto grids which were tangent to the sky at the central pointing. For each model, data were generated for 49 pointings of 60 s duration separated by $\lambda/2D$ on the sky. Most of the simulations reported on below contain no errors, so the data for each pointing have no inconsistencies, simplifying the analysis of the various reconstruction methods. At the end of this section, a few simulations are performed with pointing errors which *do* introduce inconsistencies into the data.

The error-free simulated data were imaged with a straight MOSAIC, with the AVE, LIN, and GAUSS IMERG methods, and with the first (inconsistent) UVSUB technique. The IMERG images where made with $u_1 = 8000\lambda$ ($\sim$ 10 m) and $u_2 = 25000\lambda$ ($\sim$ 32 m), the results were found to be fairly insensitive to the exact values used, but larger overlap produced slightly better results. All CLEANing was down to a maximum residual of 0.3 Jy for each field.

In all simulations performed, the GAUSS IMERG method produced the poorest results. The AVE IMERG method was limited to **DR** $\sim$ 1000, and the LIN IMERG method obtained **DR** $\sim$ 2000 for the point source simulations and a good deal higher for the resolved source simulations. Hence, only the LIN IMERG method is compared to the straight mosaic and the UVSUB method below.

Unresolved Sources. Figure 4 shows the **DR** as a function of peak surface brightness for the point source simulations. The straight mosaic performs quite well without any point sources, but as the point source strength increases, the image quality degrades rapidly as expected. The IMERG method does not perform very well either: **DR** and **FI** are nearly independent of the peak brightness and do not exceed 2000:1 and 4 respectively. Only the UVSUB method produces good images. The **DR** increases linear with peak brightness, indicating that the image quality is being limited by the deconvolution of the extended structure and not by the scaled point source. The UVSUB images have a flat **FI** around 130 for all point source strengths.

Resolved Sources. Figure 5 shows the **DR** for the simulations in which a slightly resolved Gaussian was added to the model image. IMERG performs somewhat better on resolved sources than on unresolved sources. The **DR** is below 10000:1, and the **FI** is still only about 4. UVSUB shows a linear relationship between **DR** and peak brightness, but the **DR** is lower than for the point source model. This is likely due to the larger area that is being cleaned/UVSUBed, leading to more scattered flux. UVSUB images posses a **FI** of about 40, varying only slightly with peak brightness. Straight mosaic images have very high **DR** which increases linearly with peak brightness. The **FI** ranges from 180 down to 115 for the image with highest peak

brightness.

The very high **DR** obtained from the straight mosaic images in the resolved case is a bit unrealistic because in real life the **DR** will likely be limited by pointing and primary beam errors, ie, inconsistencies between data from different pointings. It is important to recognize that UVSUBing bright point sources prior to mosaicing removes the most glaring inconsistencies in the data and enables much higher **DR** and **FI** to be achieved. The canonical 1.″2 pointing error model was applied to data generated from the model image with no point source added and also to the model image with a 300 Jy point source. When the first source was imaged with mosaic, the typical offsource rms noise was 0.05 Jy. When the data *with 300 Jy point source* was imaged with mosaic, the rms noise rose to 0.26 Jy. When the point source was imaged and removed from each field prior to mosaicing, the offsource rms decreased to 0.06 Jy. This technique will allow observations of selected sources to overcome mosaic's 1000:1 dynamic range limitation imposed by HPBW/20 pointing errors.

4 A CLEAN Based Mosaicing Algorithm

A related but purely academic topic is the possibility of a mosaicing algorithm which is based upon CLEAN rather than MEM. Equation 1 dictates how separately deconvolved CLEAN images may be corrected for the primary beam and combined into a single mosaiced image. If the data from each pointing is to be deconvolved simultaneously, a CLEAN based mosaicing algorithm might run as follows:

1. Form the linear mosaic of the dirty images from all pointings as directed by Equation 1.

2. Find the image peak, I_{peak} at $\mathbf{x}_{peak}$. Is the peak smaller than some user-specified level? If so, convolve the set of clean components with the clean beam, add residuals, and write out final image. If not, continue.

3. For each pointing, subtract $I_{peak}A(\mathbf{x}_{peak}-\mathbf{x}_p)$ times the loop gain times the point spread function, shifted to $\mathbf{x}_{peak}$, from the dirty image.

4. From the residual images for each pointing, form the linear mosaic residual image as directed by Equation 1 and return to step 2.

This mosaicing algorithm has not been implemented because the MEM based mosaic would be much more efficient for a joint deconvolution of an extended source and all advantages of the separate deconvolution found in MOSCLEAN or LTESS are lost.

5 Observational Results for NGC253

At 3.6 cm wavelength, the VLA antennas have a half power beam width of about 5′, while the nearly edge-on spiral galaxy NGC253 has a length of $\sim$ 20′ and a width of $\sim$ 4′. Observations with the VLA consisted of a single strip of seven pointings at $\lambda/2D$ separation along the major axis of NGC253 with each pointing being observed for about 1 hour. The core (0.7 Jy peak) was the brightest feature in all seven pointings, leaking in near the first null or through the first sidelobe of the primary beam for four of the seven pointings. Hence, the core was used to selfcalibrate each field prior to combining the data. When the data were imaged with MOSAIC alone, sidelobes from the bright core corrupted the faint off-core emission and limited the **DR** to about 1000:1. When a low resolution image was made with MOSAIC and a high resolution image was made with MOSCLEAN (LTESS) and the two combined in the Fourier plane with IMERG, ringing limited the **DR** to about 1000:1. The bright source in the core, a point source west of the core, and a point source northeast of the core were cleaned down to the 0.0001 Jy level and then removed from each field's data. The residual visibilities were then mosaiced using the MEM algorithm. The seven images of the bright sources which had been subtracted from the visibilities were combined in a linear mosaic and convolved with the CLEAN beam, and this image was added to the mosaic image in the image plane. The final image is shown in Figure 6. There is still a slight bowl due to missing short spacings perpendicular to the galaxy which could be improved by additional pointings to the northwest and southeast of the core, but the image is greatly improved over the image in which the fields were deconvolved separately. There is no evidence of a bowl along the length of the galaxy. The galaxy's disk, bar, and faint spiral arms can be seen. The offsource rms calculated just below the northeast spiral arm is $\sim$60 μJy, about twice thermal noise, and the dynamic range is above 10000:1. Flux from the core is scattered to the north and south due to the sidelobe pattern and the offsource rms is quite a bit higher here, but this is due to bad data rather than the mosaicing process and is a problem even with data from a single pointing.

6 Conclusions

When making very high dynamic range images, IMERG produces images with dynamic range of about 1000:1. By altering IMERG to perform a radially dependent linear weighting of the two Fourier planes, the dynamic range increases to about 2000:1, or higher if the field is dominated by resolved sources rather than point sources. However, the fidelity of such images is not very high. The original rational for IMERG was that it allows

one to perform a mosaic using only the inner 2-3 D worth of u, v data, resulting in a very large pixel size and hence a small image size for which the mosaic algorithm would take relatively little CPU time. However, for truly extended sources such as our model, the computing is dominated by accurately cleaning each field rather than by performing a high resolution mosaic. In addition, since Braun proposed the IMERG technique, the MOSAICM program in SDE has been recoded to perform minimum size FFTs, further reducing any extra cost in performing a full image mosaic to only a factor of two or three.

Using a consistent cleaning/uvsubing followed by a full resolution mosaic results in very high dynamic range ($> 10000 : 1$) and high fidelity (> 40) images when the source is dominated by one or more compact bright features. In addition, dynamic range limitations caused by pointing errors (Holdaway, 1990) and primary beam errors (Holdaway, 1992) will not apply to any compact bright features which are removed prior to the joint mosaic deconvolution.

7 Recommendations for AIPS++

Most mosaic observations will be of weak objects and will result in images which are limited by thermal noise or by spectral dynamic range. The reduction of such observations is not too difficult with currently available software; editing is fairly straightforward and no selfcalibration is required. However, some mosaic observations (such as NGC253) require high DR. Such observations require selfcalibration and careful data editing to remove bad data. The selfcalibration and editing of the seven pointings on NGC253 at X band took about a week of Chris Carilli's hard work. Such care in data reduction is not currently feasible for a 100 pointing mosaic. What is required is an automated editing and selfcalibration program which can deal with many pointings simultaneously. Such a program is absolutely required for the proposed Millimeter Array, which will perform very large mosaics (100-1000 pointings) routinely.

8 References

Braun, R. (1988), MMA Memo 46, *Mosaicing with High Dynamic Range.*
Braun, R. (1989), MMA Memo 54, *Simulations of Primary Beam Truncation and Pointing Errors with the MMA.*
Holdaway, M.A. (1990), MMA Memo 61, *Imaging Characteristics of a Homogeneous Millimeter Array.*

Holdaway, M.A. (1992), MMA Memo 74, *Required Surface Accuracy for the MMA Antennas.*
Cornwell, T.J., Holdaway, M.A., and Uson, J. (1992) *A. A., in preparation.*
Narayan, R. and Nityananda, R. (1986), *Ann. Rev. Atron. Atrophys.*, **24**, p 127.

Figure 1: Illustration of the different IMERG averaging schemes.

Figure 2: Dynamic range as a function of CLEAN stopping flux.

Figure 3: Steps involved in subtracting clean components consistently from multiple pointing data.

Figure 4: Dynamic range as a function of peak brightness of model image (a scaled *point source* added to the M31 HII region model image) for the LIN IMERG, straight MOSAIC, and UVSUB/MOSAIC methods.

Figure 5: Dynamic range as a function of peak brightness of model image (a scaled 4″ *Gaussian* added to the M31 HII region model image) for the LIN IMERG, straight MOSAIC, and UVSUB/MOSAIC methods.

Figure 6: Seven pointing VLA mosaic image of the nearly edge-on spiral galaxy NGC253. Dynamic range is about 10000:1.

AVE

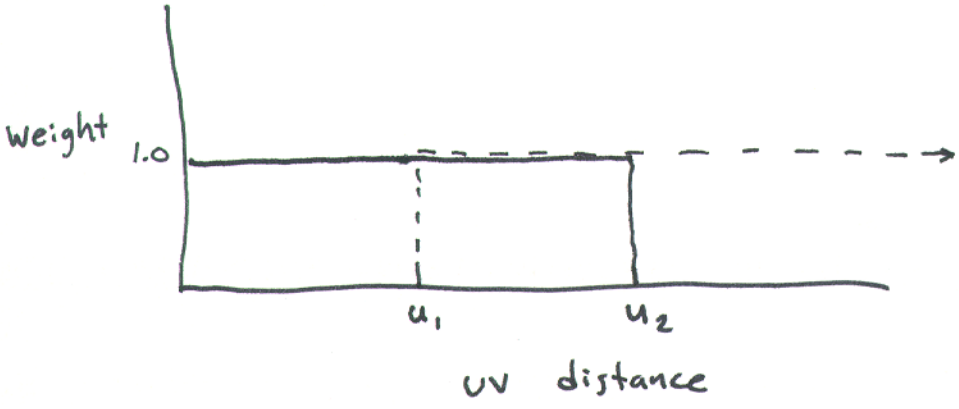

LIN

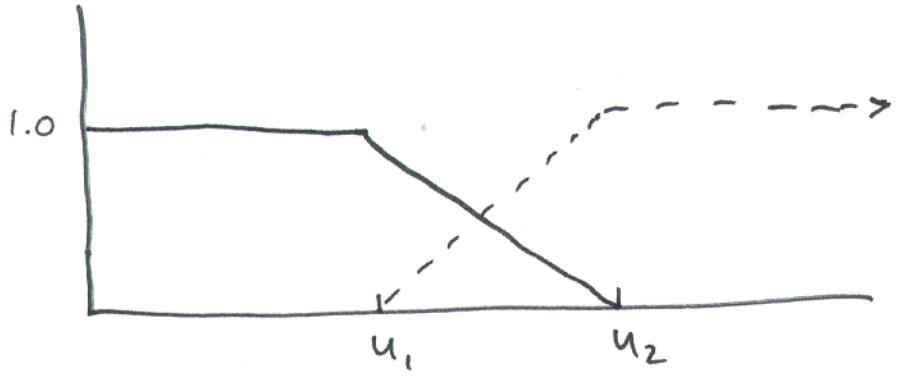

GAUSS

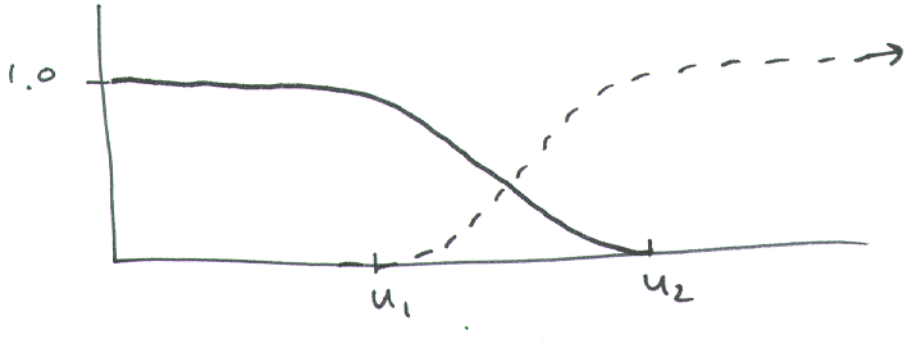

Figure 1

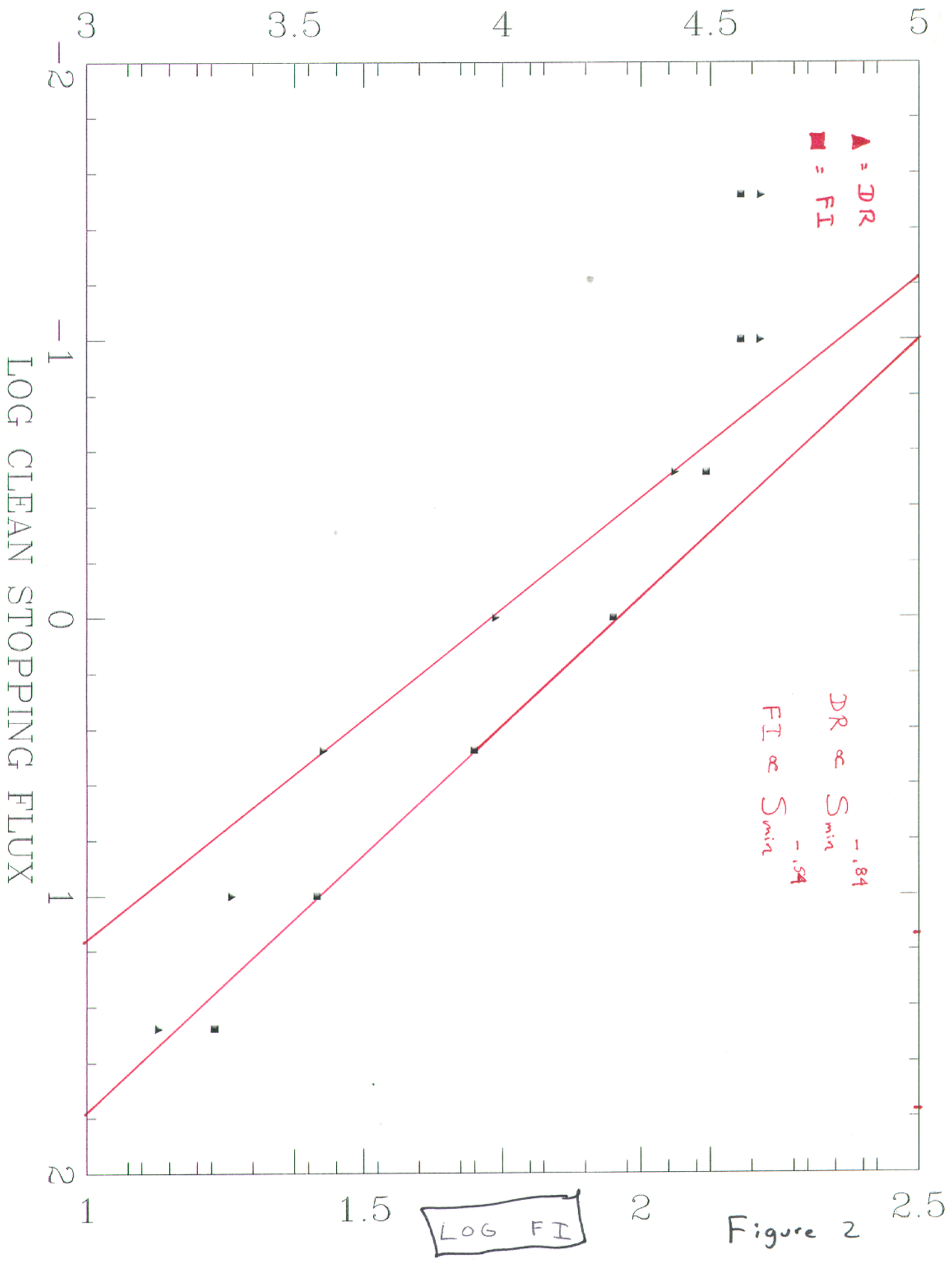
LOG DYNAMIC RANGE
3
3.5
4
4.5
5
−2
−1
0
1
2
LOG CLEAN STOPPING FLUX
▲ = DR
■ = FI
DR & S_{min} -.84
FI & S_{min} -.84
1
1.5
2
2.5
LOG FI

Figure 2

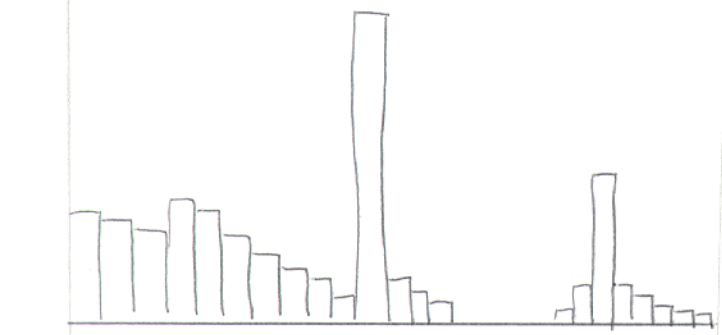

(a) Clean Components, cleaned down to ϵ

residual $\sim \epsilon$ for all pixels

(b) Clean Components selected to be subtracted from u-v data

residuals $\sim \epsilon$

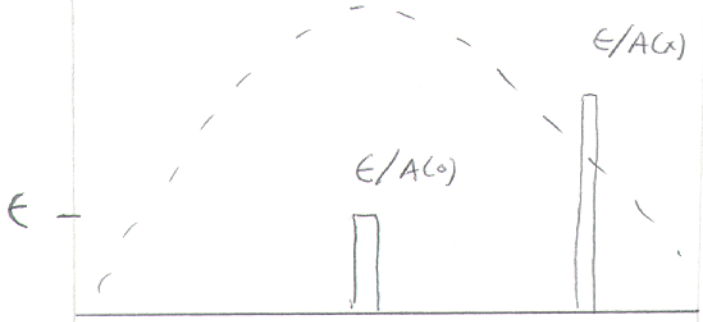

(c) Primary beam and level of residuals after dividing by the primary beam

Figure 3

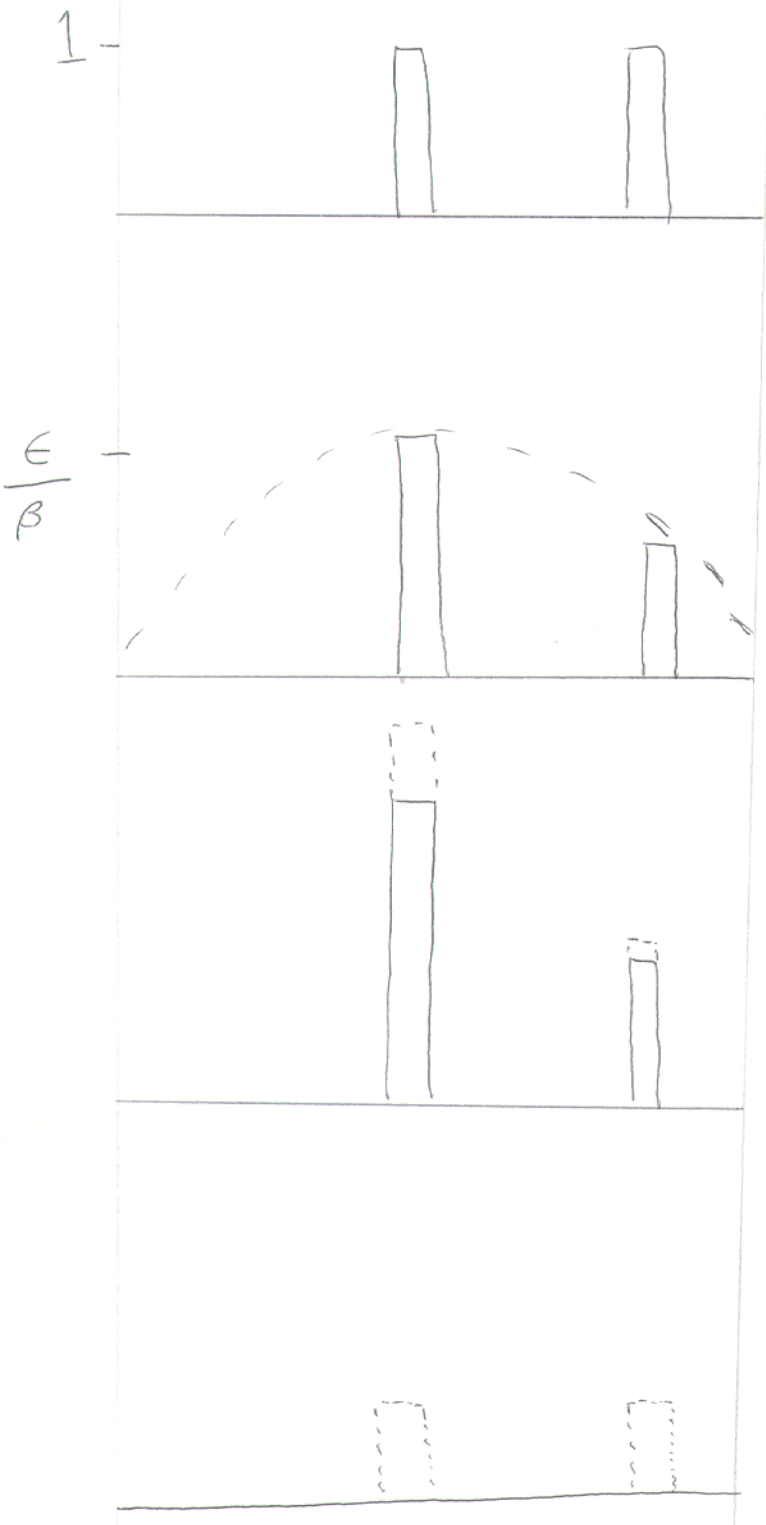

(d) Unit Mast of Clean Components selected to be subtracted

(e) Unit Mask times $A(x) \cdot \frac{\epsilon}{\beta}$ where $\beta \sim .2$

(f) Subtract $A(x) \cdot \frac{\epsilon}{\beta} - \epsilon$ from clean components

(g) Residual before dividing by $A(x)$ is $\sim A(x)\frac{\epsilon}{\beta}$

After correcting by $A(x)$, residual is $\sim \frac{\epsilon}{\beta}$

Figure 3 (cont)

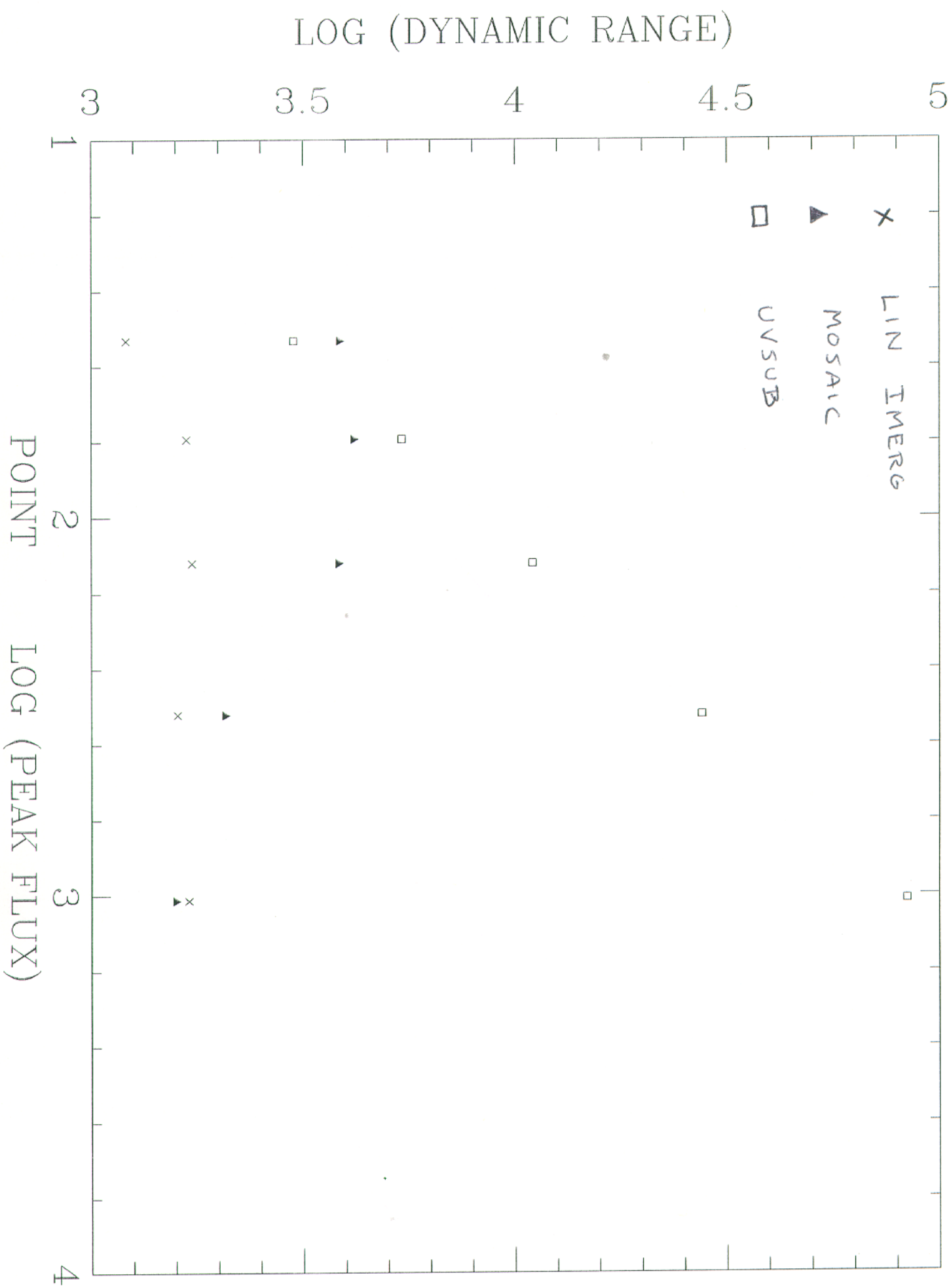
LOG (DYNAMIC RANGE)
3
3.5
4
4.5
5
1
2
3
4
LOG (PEAK FLUX)
POINT
LIN IMERG
MOSAIC
UVSUB

Figure 4

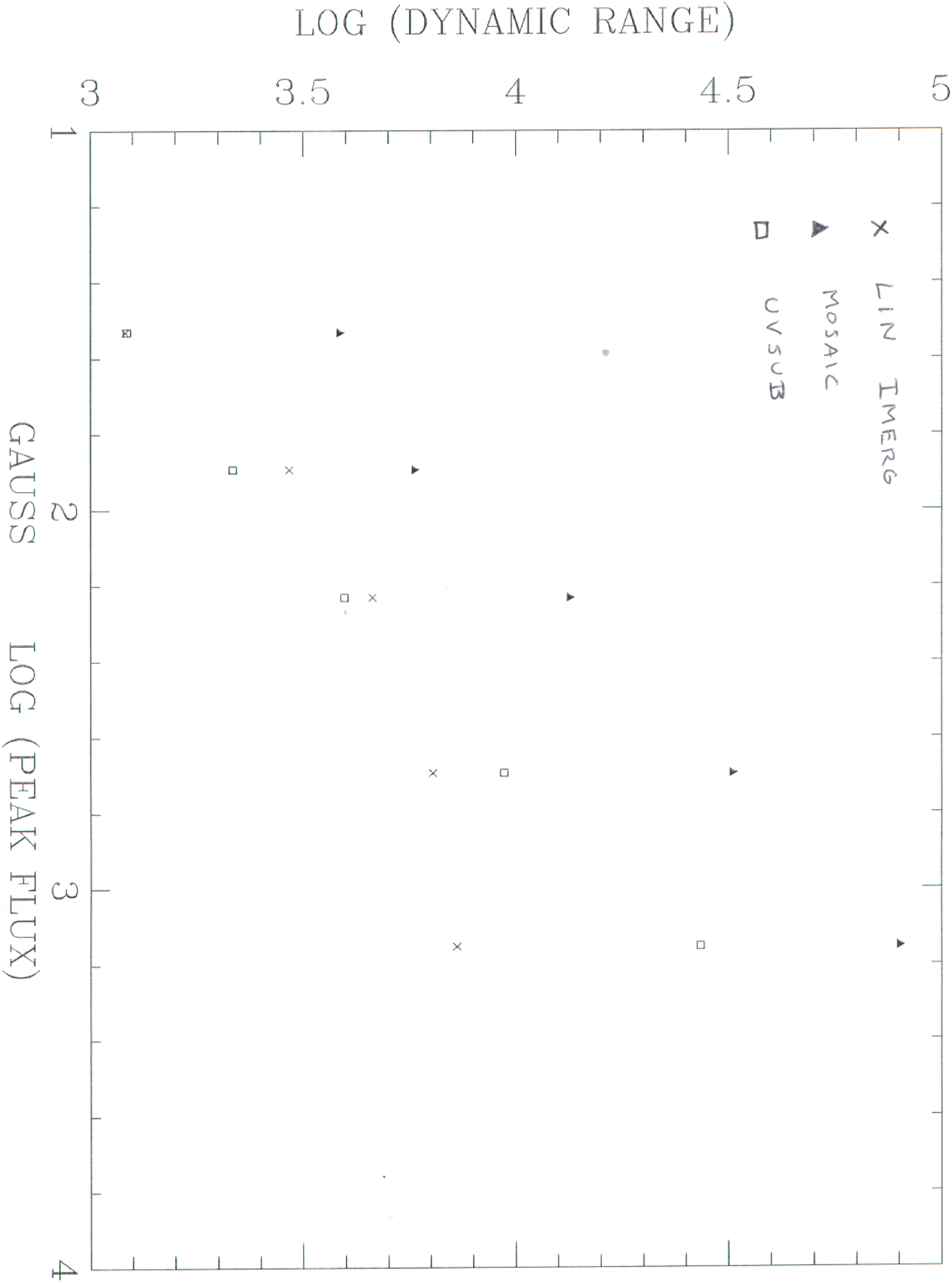
LOG (DYNAMIC RANGE)
3
3.5
4
4.5
5
1
2
3
4
GAUSS LOG (PEAK FLUX)
LIN IMERG
MOSAIC
UVSUB

Figure 5

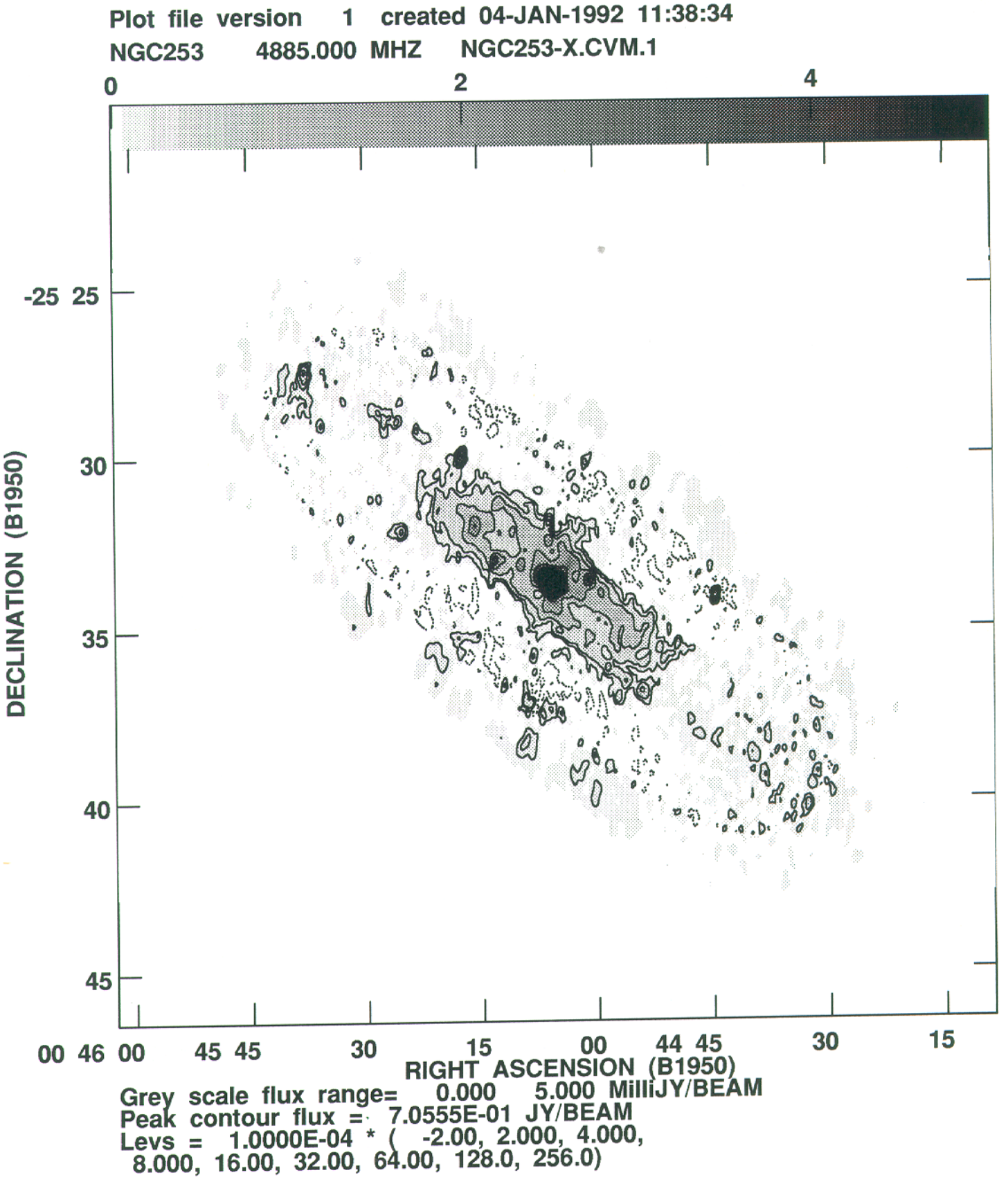
Plot file version 1 created 04-JAN-1992 11:38:34
NGC253 4885.000 MHZ NGC253-X.CVM.1
0
2
4
-25 25
30
35
40
45
DECLINATION (B1950)
00 46 00
45 45
30
15
00
44 45
30
15
RIGHT ASCENSION (B1950)
Grey scale flux range= 0.000 5.000 MilliJY/BEAM
Peak contour flux = 7.0555E-01 JY/BEAM
Levs = 1.0000E-04 * (-2.00, 2.000, 4.000,
8.000, 16.00, 32.00, 64.00, 128.0, 256.0)

Figure 6